SIMULATION OF FLIGHT CONTROL OF A HUMMINGBIRD LIKE ROBOT NEAR HOVER

M. Karásek, A. Preumont [*]

Abstract: *Interest in Micro Air Vehicles (MAVs) capable of hovering is gradually increasing because they can be a low-cost solution for security applications or remote inspection. Much research has centred on designs inspired by insects and hummingbirds, where the propellers are replaced by flapping wings. It is assumed that that flapping wings improve, at small scales, both manoeuvrability and energy efficiency. This numerical work based on quasi-steady aerodynamics applies to a hummingbird robot with a pair of flapping wings and a 12 cm wingspan. We construct a control derivatives matrix that estimates the effect of each wing kinematics parameter on the cycle averaged wing forces and forms the key stone of the flight controller. We implement the controller in a simulation model with rigid body dynamics and "continuous" (i.e. not averaged) aerodynamics. The simulation results show that the controller stabilizes the robot attitude and controls the flight in 4 DOF (translation in any direction + yaw rotation) by modifying only 2 wing kinematic parameters per wing - the flapping amplitude and the mean wing position. Other control parameters are possible. Thus, various mechanical design solutions can be studied in the future.*

Keywords: *Micro Air Vehicle, flapping wings, control.*

1. Introduction

Micro Air Vehicles (MAVs) are small flying robots with remote or autonomous operation designed to fly indoors or outdoors. They are being used by private companies as well as law enforcement units for aerial photography, terrain reconnaissance and video surveillance. A vast majority of MAVs is based on fixed and rotary wings.

MAVs with flapping wings have been researched intensively during recent years. These bio-inspired designs mimicking hummingbirds and insects are believed to combine energy efficient lift production, capability of hovering flight and high maneuverability. First successful flapping wing MAVs had dragonfly morphology (de Croon et al., 2009), see Fig. 1 left. Nano Hummingbird (Keennon et al., 2012) is the first man-made flapping wing MAV to take-off, hover and fly in any direction. The researchers managed to integrate avionics, flapping and control mechanisms and a battery sufficient for 11 min flight into a robot of 19 g with 16.5 cm wingspan (Fig. 1 right).
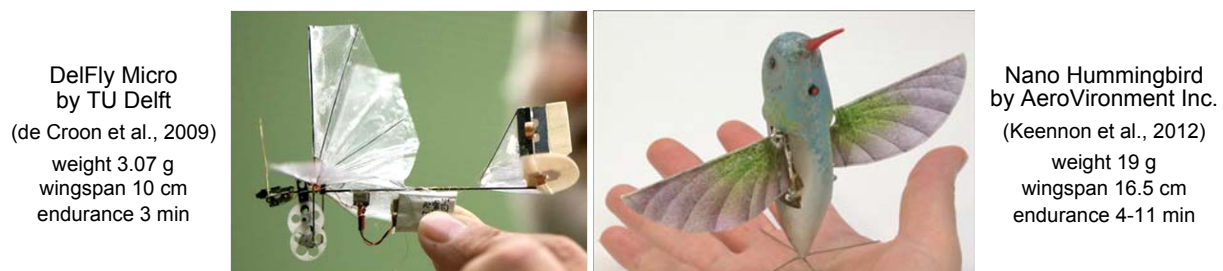

DelFly Micro
by TU Delft
(de Croon et al., 2009)
weight 3.07 g
wingspan 10 cm
endurance 3 min

Nano Hummingbird
by AeroVironment Inc.
(Keennon et al., 2012)
weight 19 g
wingspan 16.5 cm
endurance 4-11 min

Fig. 1: Examples of MAVs with flapping wings

Characteristic features of flapping flight include high flapping frequencies (from 15 Hz in large hummingbirds to hundreds of Hz in insects) and high angles of attack. The aerodynamic mechanisms of

[*]Ing. Matěj Karásek, Prof. André Preumont: Active Structures Laboratory, Université Libre de Bruxelles, CP 165/42, Av.F.D.Roosevelt 50; 1050, Brussels; BE, e-mail: matej.karasek@ulb.ac.be

flapping wings responsible for high lift production were described in (Sane, 2003; Shyy et al., 2010). Studies on flapping flight stability and control mechanisms, recently reviewed by (Orlowski & Girard, 2012), show that the flapping flight is naturally unstable. It is controlled by modifications of wing trajectory.

Many simulations of flapping flight have been carried out, the majority of them uses quasi-steady aerodynamics derived from thin airfoil theory using blade elements theory (Sane & Dickinson, 2002). Various control approaches were successfully used: pseudo-inverse allocation + PID (Orlowski et al., 2010), output-feedback LQR (Deng et al., 2006a,b), back-stepping and feedback linearization (Rakotomamonjy et al., 2010) or Central Pattern Generator control that mimicks spinal cords (Chung & Dorothy, 2010).

In this numerical work, based on quasi-steady aerodynamics and rigid body dynamics, we present a control strategy that is similar to cascade control of quadrocopters (Michael et al., 2010). Flight is controlled in 4 DOF (any direction + turning); vertical flight and turning is controlled directly, while flight forward/backward and sideways is achieved by body pitching and rolling respectively. We parametrize the wing kinematics and study the effect of each parameter on cycle averaged forces and moments generated by the wing. From the results we construct a control derivatives matrix (similar to (Doman et al., 2010)), that is used to transform the control forces/moments into wing motion changes. We discuss the selection of control parameters as these are crucial for design of wing mechanism in future robot. Finally we test the control performance with a selected set of control parameters in simulation.

2. Mathematical model

2.1. Wing motion

Motion of a flapping wing can be described by 3 angles (Fig. 2): sweep angle ϕ, deviation angle δ and wing inclination angle α^*. They are measured from the mean stroke plane, which is inclined from the body horizontal plane $x_B y_B$ by Θ.
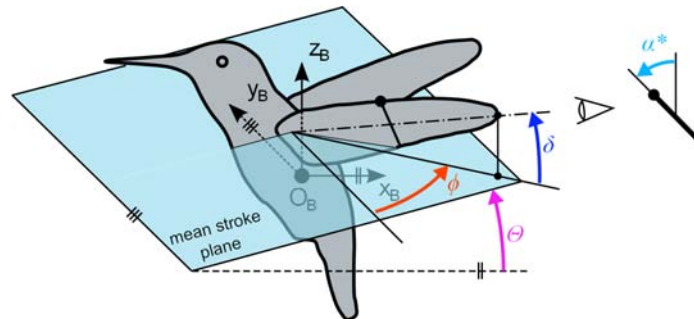

Fig. 2: Wing motion angles: sweep angle ϕ, deviation angle δ and inclination angle α^*

In the current study we assume harmonic motion in all three DOFs according to equations

$$\phi = \phi_0 + \phi_m cos(2\pi f t)$$
$$\alpha^* = \alpha_0 + (\pi/2 - \alpha_m)sin(2\pi f t - \varphi_\alpha)$$
$$\delta = \begin{cases} \delta_{m1}sin(2\pi f t) \\ \delta_{m2}sin(4\pi f t) \end{cases} \tag{1}$$

where t is time. The motion is parameterized by 9 parameters (Fig. 3): flapping frequency f, mean stroke plane angle Θ, sweep angle amplitude ϕ_m and offset ϕ_0; inclination angle amplitude α_m, offset α_0 and phase shift φ_α; deviation angle amplitude δ_{m1} (resulting into an oval trajectory) or δ_{m2} (resulting into a "figure 8" trajectory).

2.2. Quasi-steady aerodynamics

We use quasi steady approach (Sane & Dickinson, 2002) to model the forces generated by flapping wings. The wing is assumed to be flat and rigid. The model was derived from steady flow thin airfoil
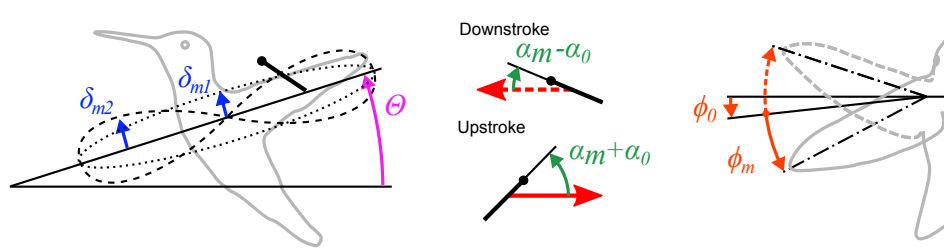
Fig. 3: Wing motion angles: sweep angle ϕ, deviation angle δ and angle of attack α

theory using blade element theory. Experimentally obtained force coefficients published by (Dickinson et al., 1999) include, at least partially, the effects of "unsteady" flow mechanisms typical for flapping flight.

We consider two force components: translational force and rotational force. Because they result mainly from pressure field distribution around the wing they are placed to the center of pressure (CP). We neglect the effect of added mass inertia of the surrounding fluid (virtual mass force) as its contribution to the total force is very small.

The necessary wing geometry parameters are displayed in Fig. 4, definitions are given in (Ellington, 1984). S is the surface of a single wing, R is the wing length, $\bar{c}$ is the mean chord length, $\hat{r} = r/R$ is non-dimensional position of a wing blade and $\hat{c} = c/\bar{c}$ is the normalized chord length, $\hat{x}_0$ is the non-dimensional position of the rotational axis. Similar to other studies we assume the center of pressure (CP) is located, in chord-wise direction, at the rotational axis. The span-wise CP location R_{CP} is determined by the product of wing length R and the radius of second moment of inertia $\hat{r}_2$.
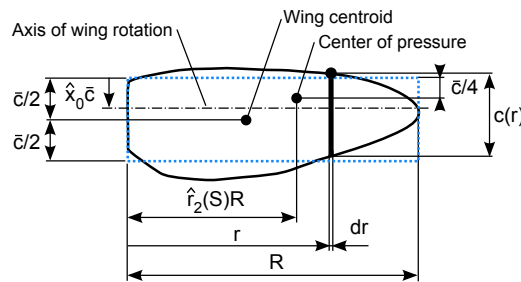

Fig. 4: Wing geometry parameters

According to (Deng et al., 2006a) the total force can be expressed, in normal and tangential direction of the wing, as

$$F_{T,tr} = 0.5\rho S U_{CP}^2 C_T(\alpha)$$

$$F_{N,tr} = 0.5\rho S U_{CP}^2 C_N(\alpha) + \pi \left(\frac{3}{4} - \hat{x}_0\right) \rho \dot{\alpha} \frac{U_{CP}}{\hat{r}_2} \bar{c}^2 R \int_0^1 \hat{r}\hat{c}^2(\hat{r})d\hat{r} \tag{2}$$

where ρ is the air density and $C_N(\alpha)$ and $C_T(\alpha)$ are the force coefficients given as a function of angle of attack α by expressions

$$C_N(\alpha) = 3.4\sin(\alpha)$$

$$C_T(\alpha) = \begin{cases} 0.4\cos^2(2\alpha) & 0 \le |\alpha| < \frac{\pi}{4} \\ 0 & \frac{\pi}{4} \le |\alpha| < \frac{3\pi}{4} \\ -0.4\cos^2(2\alpha) & \frac{3\pi}{4} \le |\alpha| < \pi \end{cases} \tag{3}$$

2.3. Center of pressure velocity and angle of attack

To express the CP velocity we introduce three coordinate frames: global frame G, body-fixed frame B and wing-fixed frame W. They are displayed in Fig. 5. A left superscript is used to indicate the frame in

which a vector or matrix is expressed. The CP velocity is a resultant of body absolute motion (velocity $\mathbf{v_{GB}}$, angular velocity $\boldsymbol{\omega_{GB}}$) and the wing rotation around the body (angular velocity $\boldsymbol{\omega_{BW}}$). Using the simultaneous motion theory we can express the velocity of CP in W frame as

$$^{\mathbf{W}}\mathbf{v_{GCP}} = \mathbf{R_{WB}} \left({}^{\mathbf{B}}\mathbf{v_{GB}} + {}^{\mathbf{B}}\boldsymbol{\omega_{GB}} \times {}^{\mathbf{B}}\mathbf{r_{BCP}} \right) + {}^{\mathbf{W}}\boldsymbol{\omega_{BW}} \times {}^{\mathbf{W}}\mathbf{r_{WCP}} \tag{4}$$

where $\mathbf{r_{WCP}}$ and $\mathbf{r_{BCP}}$ is the CP position in the wing frame and in the body frame respectively. $\mathbf{R_{WB}}$ is the matrix of rotation from wing frame to body frame (given by wing position angles ϕ, δ and α^*).
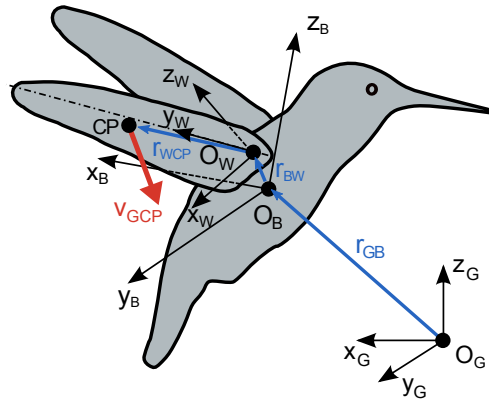

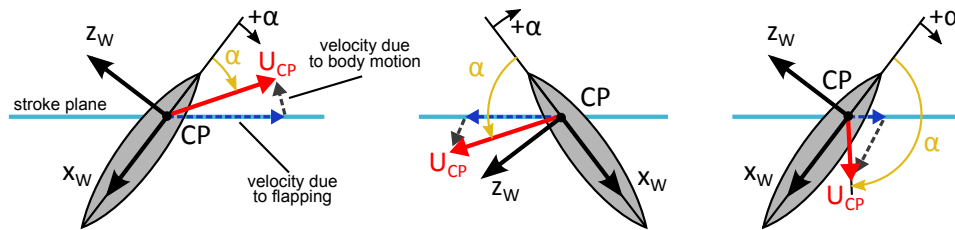*Fig. 5: Coordinate frames and center of pressure velocity*

Fig. 6: Angle of attack in various situations

The angle of attack is measured between the wing chord and the velocity vector of the wing. Since not only the magnitude but also the direction of CP velocity changes, the aerodynamic angle of attack is also affected as can be seen in Fig. 6. Situations, where angle of attack is negative or greater than $90°$ are also sketched. The magnitude of the CP velocity vector in $x_W z_W$ plane of the wing is

$$U_{CP} = \sqrt{{}^{W}v_{GCPx}^2 + {}^{W}v_{GCPz}^2} \tag{5}$$

According to Fig. 6 the angle of attack can be computed as

$$\alpha = \mathrm{atan2}(-{}^{W}v_{GCPz}, -{}^{W}v_{GCPx}) \tag{6}$$

where the atan2 function returns values between $-\pi$ and π.

2.4. Body dynamics

The dynamics of the flying robot can be described, under rigid body assumption, by Newton-Euler motion equations. Similar to an aircraft (e.g. (Padfield, 2007)) we obtain 12 ordinary differential equations with 12 unknown coordinates - velocity (u, v, w), angular velocity (p, q, r), position (x, y, z) and orientation expressed by Roll-Pitch-Yaw angles $(\varphi, \vartheta, \psi)$ - see Fig.7. By omitting the equations for position

and heading (yaw) angle ψ the system is reduced to 8 equations

$$\dot{u} = -(wq - vr) + X/m + g\sin\vartheta$$
$$\dot{v} = -(ur - wp) + Y/m - g\cos\vartheta\sin\varphi$$
$$\dot{w} = -(vp - uq) + Z/m - g\cos\vartheta\cos\varphi$$
$$I_{xx}\dot{p} = (I_{yy} - I_{zz})\,qr + I_{xz}\,(\dot{r} + pq) + L$$
$$I_{yy}\dot{q} = (I_{zz} - I_{xx})\,pr + I_{xz}\,(r^2 - p^2) + M$$
$$I_{zz}\dot{r} = (I_{xx} - I_{yy})\,pq + I_{xz}\,(\dot{p} - qr) + N$$
$$\dot{\varphi} = p + q\sin\varphi\tan\vartheta + r\cos\varphi\tan\vartheta$$
$$\dot{\vartheta} = q\cos\varphi - r\sin\varphi \tag{7}$$

where m is the body mass. I_{xx}, I_{yy}, I_{zz} and I_{xz} are the non-zero moments and product of inertia in body frame (products I_{xy} and I_{yz} are both zero due to body symmetry). Aerodynamic forces and moments are represented by vectors (X, Y, Z) and (L, M, N) respectively.
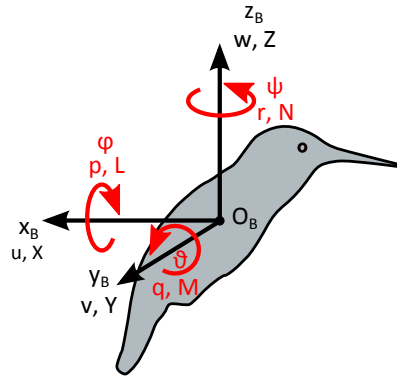

Fig. 7: Definition of body coordinates

We transform the wing forces (2) into body frame as follows

$$[X, Y, Z]^T = \sum_i [X_i, Y_i, Z_i]^T = \sum_i \mathbf{R_{BWi}}\,[F_{Ti}, 0, F_{Ni}]^T \tag{8}$$

$$[L, M, N]^T = \sum_i {}^{\mathbf{B}}\mathbf{r_{BCP_i}} \times [X_i, Y_i, Z_i]^T \tag{9}$$

where index i stands for the left and the right wing. $\mathbf{R_{BW}}$ is the transformation matrix from B frame to W frame ($\mathbf{R_{BW}} = \mathbf{R_{WB}}^T$) and ${}^{\mathbf{B}}\mathbf{r_{BC}}$ is the CP (force application point) position expressed in the body frame as

$$^{\mathbf{B}}\mathbf{r_{BC}} = {}^{\mathbf{B}}\mathbf{r_{BW}} + \mathbf{R_{BW}}\,{}^{\mathbf{W}}\mathbf{r_{WCP}} \tag{10}$$

with ${}^{\mathbf{B}}\mathbf{r_{BW}} = [\pm w/2, 0, l_1]^T$ defining the position of the right/left wing base in the body frame and ${}^{\mathbf{W}}\mathbf{r_{WCP}} = [0, \pm R_{CP}, 0]^T$ defining the CP position inside the right/left wing frame.

2.5. System linearization

The mathematical model introduced in previous sections is nonlinear and was used in simulations. For control design a linear model is preferred.

The system dynamics (7) include aerodynamic forces and moments (8-9) that are functions of wing motion parameters $\mathbf{p} = [f, \Theta_L, \phi_{mL}, \phi_{0L}, \alpha_{mL}, \alpha_{0L}, \varphi_{\alpha L}, \delta_{m1L}, \delta_{m2L}, \Theta_R, \cdots, \delta_{m2R}]^T$, system state $\mathbf{x} = [u, v, w, p, q, r, \varphi, \vartheta]^T$ and time t. Assuming the flapping frequency is much higher than the bandwidth of the system, the aerodynamic forces can be replaced by their cycle averaged values (mean values over one wingbeat), e.g.

$$\overline{X} = \int_0^{\frac{1}{f}} X(\mathbf{x}, \mathbf{p}, t)\mathrm{d}t = \overline{X}(\mathbf{x}, \mathbf{p}) \tag{11}$$

that depend only on **x** and **p**. We use small perturbation theory to rewrite the states and wing motion parameters as

$$\mathbf{x} = \mathbf{x_e} + \delta\mathbf{x}, \quad \mathbf{p} = \mathbf{p_e} + \delta\mathbf{p} \tag{12}$$

where subscript e signifies the equilibrium values and δ is the perturbation. We approximate the aerodynamic forces and moments by the linear terms of Taylor's expansion. For force in x-axis we obtain

$$\overline{X}(\mathbf{x}, \mathbf{p}) = \overline{X}_e(\mathbf{x_e}, \mathbf{p_e}) + \sum_{i=1}^{6} \frac{\partial \overline{X}}{\partial x_i} \delta x_i + \sum_{j=1}^{n} \frac{\partial \overline{X}}{\partial p_j} \delta p_j \tag{13}$$

where $\overline{X}_e$ is the cycle averaged force generated in equilibrium and n is number of wing kinematic parameters. The terms of the first summation are the derivatives with respect to body velocities and angular velocities called the stability derivatives. If taken with an opposite sign they represent aerodynamic damping. The second summation terms are the derivatives with respect to changes in wing motion. They are called the control derivatives. Further the overbar notation for cycle averages is dropped and the notation of the derivatives is shortened in the following manner

$$\frac{\partial \overline{X}}{\partial u} = X_u, \quad \frac{\partial \overline{X}}{\partial v} = X_v, \quad \ldots \quad, \quad \frac{\partial \overline{X}}{\partial f} = X_f, \quad \frac{\partial \overline{X}}{\partial \Theta} = X_\Theta, \quad \ldots \tag{14}$$

In this study we consider only near hover flight. Thus, all the equilibrium states are zero ($u_e = v_e = w_e = p_e = q_e = r_e = \varphi_e = \vartheta_e = 0$) and the perturbed states are equal to their absolute values ($\delta\mathbf{x} = \mathbf{x}$). The wing motion parameters $\mathbf{p_e}$ must ensure the trim: the z-force must be in balance with the gravity force ($Z_e = mg$), while the remaining forces and moments need to be zero ($X_e = Y_e = L_e = M_e = N_e = 0$).

First we suppose the wing kinematics does not change ($\delta\mathbf{p} = \mathbf{0}$). Instead, we assume we can apply an arbitrary external force or moment on the body. According to previous works on passive stability (Taylor & Thomas, 2002; Taylor et al., 2003; Zhang & Sun, 2010) as well as to our results there exists no aerodynamic coupling between the longitudinal and lateral system. By neglecting second order terms, we can rewrite the equations as two linear subsystems represented in state space as

$$\left[\dot{u}, \dot{w}, \dot{q}, \dot{\vartheta}\right]^T = \mathbf{A_{long}} \left[u, w, q, \vartheta\right]^T + \mathbf{B_{long}}[X, Z, M]^T$$
$$\left[\dot{v}, \dot{p}, \dot{r}, \dot{\varphi}\right]^T = \mathbf{A_{lat}} \left[v, p, r, \varphi\right]^T + \mathbf{B_{lat}}[Y, L, N]^T \tag{15}$$

where the system and control matrices, **A** and **B**, are expressed as

$$\mathbf{A_{long}} = \begin{bmatrix} \frac{X_u}{m} & \frac{X_w}{m} & \frac{X_q}{m} & g \\ \frac{Z_u}{m} & \frac{Z_w}{m} & \frac{Z_q}{m} & 0 \\ \frac{M_u}{I_{yy}} & \frac{M_w}{I_{yy}} & \frac{M_q}{I_{yy}} & 0 \\ 0 & 0 & 1 & 0 \end{bmatrix}, \quad \mathbf{A_{lat}} = \begin{bmatrix} \frac{Y_v}{m} & \frac{Y_p}{m} & \frac{Y_r}{m} & -g \\ \frac{L_v I_{zz} + N_v I_{xz}}{I_{xx} I_{zz} - I_{xz}^2} & \frac{L_p I_{zz} + N_p I_{xz}}{I_{xx} I_{zz} - I_{xz}^2} & \frac{L_r I_{zz} + N_r I_{xz}}{I_{xx} I_{zz} - I_{xz}^2} & 0 \\ \frac{L_v I_{xz} + N_v I_{xx}}{I_{xx} I_{zz} - I_{xz}^2} & \frac{L_p I_{xz} + N_p I_{xx}}{I_{xx} I_{zz} - I_{xz}^2} & \frac{L_r I_{xz} + N_r I_{xx}}{I_{xx} I_{zz} - I_{xz}^2} & 0 \\ 0 & 1 & 0 & 0 \end{bmatrix}$$

$$\mathbf{B_{long}} = \begin{bmatrix} \frac{1}{m} & 0 & 0 \\ 0 & \frac{1}{m} & 0 \\ 0 & 0 & \frac{1}{I_{yy}} \\ 0 & 0 & 0 \end{bmatrix}, \quad \mathbf{B_{lat}} = \begin{bmatrix} \frac{1}{m} & 0 & 0 \\ 0 & \frac{I_{zz}}{I_{xx} I_{zz} - I_{xz}^2} & \frac{I_{xz}}{I_{xx} I_{zz} - I_{xz}^2} \\ 0 & \frac{I_{xz}}{I_{xx} I_{zz} - I_{xz}^2} & \frac{I_{xx}}{I_{xx} I_{zz} - I_{xz}^2} \\ 0 & 0 & 0 \end{bmatrix} \tag{16}$$

In the following section a controller will be designed, assuming the external forces and moments as inputs. In reality, these will be generated by the wings. From the approximation in (13) we can write a relation between cycle averaged forces/moments and modifications of wing kinematics parameters $\mathbf{\Delta p}$ as

$$[X, Y, Z, L, M, N]^T = \mathbf{J}\Delta\mathbf{p} \tag{17}$$

where $\mathbf{J}$ is the matrix of control derivatives defined as

$$\mathbf{J} = \begin{bmatrix} X_{p_1} & X_{p_2} & \cdots & X_{p_n} \\ Y_{p_1} & Y_{p_2} & \cdots & Y_{p_n} \\ \vdots & \vdots & \ddots & \vdots \\ N_{p_1} & N_{p_2} & \cdots & N_{p_n} \end{bmatrix} \tag{18}$$

The kinematic parameters modifications that should produce desired forces/moments are estimated by a pseudoinverse of the previous relation

$$\mathbf{\Delta p} = \mathbf{J}^+[X, Y, Z, L, M, N]^T \tag{19}$$

3. Control design

In the previous section we have presented the complete mathematical model which is necessary to perform an open loop simulation. The next task is to develop a 4DOF flight controller, allowing us to fly foreward/backward, up/down and sideways and to steer by changing the heading angle. As we show further the system itself is unstable. Thus, the controller also needs to stabilize the attitude.

This section applies to a robot with wing and body properties of a typical hummingbird (Tab.1,2). We take the mass of a ruby-throated hummingbird (Chai et al., 1996) and estimate the inertia and wing base position according to a simplified 3D model in Catia with typical body dimensions. We used Matlab image processing to obtain the wing geometry parameters from an image of a real hummingbird wing profile (Fig. 8). Wing kinematic parameters for equilibrium (i.e. hover) $\mathbf{p_e}$ are in Tab. 3. They were chosen to satisfy the trim condition with a relative error below 0.5% while being close to real animal observations (Tobalske et al., 2007).

Tab. 1: Aerodynamic parameters

R (mm)	$\bar{c}$ (mm)	S (mm^2)	$\hat{x}_0$ (-)	$\int_0^1 \hat{r}\hat{c}^2(\hat{r})d\hat{r}$ (-)	$\hat{r}_2$ (-)	ρ (kg.m^{-3})
48	12.7	611	0.25	0.428	0.492	1.2

Tab. 2: Body parameters

m (g)	I_{xx} (g.mm^2)	I_{yy} (g.mm^2)	I_{zz} (g.mm^2)	I_{xz} (g.mm^2)	l_1 (mm)	w (mm)
4.32	492	557	411	-220	10	14

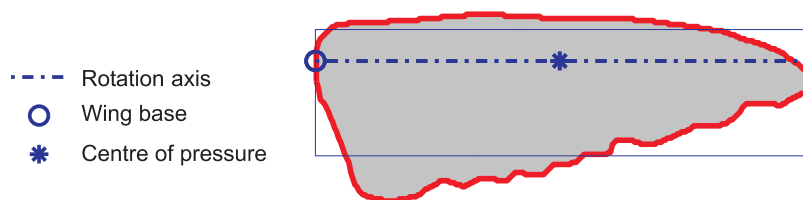- – · – Rotation axis
- ○ Wing base
- ✳ Centre of pressure

Fig. 8: Hummingbird wing profile

3.1. System matrices

We evaluate the stability derivatives in hover as follows. We keep the wing kinematics constant and symmetric for both wings ($\mathbf{p_e}$). We pick several values of one of the velocities from a defined neighborhood around zero while keeping the others in zero. In each case we calculate the vector of cycle averaged forces and moments in body frame. The relationships between the averaged forces/moments and the

Tab. 3: Wing kinematics for hover

f (Hz)	Θ (°)	ϕ_m (°)	ϕ_0 (°)	α_m (°)	α_0 (°)	φ_α (°)	δ_{m1} (°)	δ_{m2} (°)
48	0	70	0	30	0	0	0	0

varying velocity can be plotted - the derivatives are represented by a tangent to the curves in the origin. We proceed similarly to get the derivatives with respect to the remaining velocities. We find out that many of them are zero, so we only keep X_u, X_q, Y_v, Y_p, Z_w, L_v, L_p, M_u, M_q and N_r. This justifies splitting the system into longitudinal and lateral part. It further reveals that vertical translation and yaw rotation are aerodynamically decoupled from the remaining motions.

The expressions in the system matrices reduce to

$$
\mathbf{A_{long}} = \begin{bmatrix} \frac{X_u}{m} & 0 & \frac{X_q}{m} & g \\ 0 & \frac{Z_w}{m} & 0 & 0 \\ \frac{M_u}{I_{yy}} & 0 & \frac{M_q}{I_{yy}} & 0 \\ 0 & 0 & 1 & 0 \end{bmatrix}, \quad
\mathbf{A_{lat}} = \begin{bmatrix} \frac{Y_v}{m} & \frac{Y_p}{m} & 0 & -g \\ \frac{L_v I_{zz}}{I_{xx}I_{zz}-I_{xz}^2} & \frac{L_p I_{zz}}{I_{xx}I_{zz}-I_{xz}^2} & \frac{N_r I_{xz}}{I_{xx}I_{zz}-I_{xz}^2} & 0 \\ \frac{L_v I_{xz}}{I_{xx}I_{zz}-I_{xz}^2} & \frac{L_p I_{xz}}{I_{xx}I_{zz}-I_{xz}^2} & \frac{N_r I_{xx}}{I_{xx}I_{zz}-I_{xz}^2} & 0 \\ 0 & 1 & 0 & 0 \end{bmatrix} \tag{20}
$$

In the longitudinal system a vertical motion is fully decoupled from the rest. In the lateral system all three motions are coupled. While the sideways motion and roll are coupled aerodynamically, yaw and roll are coupled due to non-zero inertia product I_{xz}. Thus, it would be possible to avoid this coupling by designing a robot with mass distribution that would be symmetrical around all the three body axes.

Calculation of system poles gives results that are in accordance with previous stability studies (reviewed in (Orlowski & Girard, 2012)). Both systems, longitudinal and lateral, have similar pole structure resulting into one unstable oscillatory natural mode and two (fast and slow) stable natural modes and need to be stabilized.

3.2.   Control strategy

We have shown in the preceding section that the system can be split into 3 decoupled subsystems - longitudinal dynamics (u,q), vertical dynamics (w) and lateral + yaw dynamics (v,p,r). Moreover, lateral and yaw dynamics are coupled by inertia product I_{xz} - there is no aerodynamic coupling. We can take an advantage of this decoupling and use a decentralized cascade control strategy similar to quadrocopters (Michael et al., 2010). The controller is formed by two loops. An inner loop is stabilizing the attitude (roll φ and pitch ϑ) by respective moments L, M. An outer loop controls the flight. Flying up/down and turning is controlled directly by Z force and N moment. Forwards/backwards and sideways flight is controlled indirectly by body inclination around pitch and roll axis. The controller scheme is in Fig. 9.
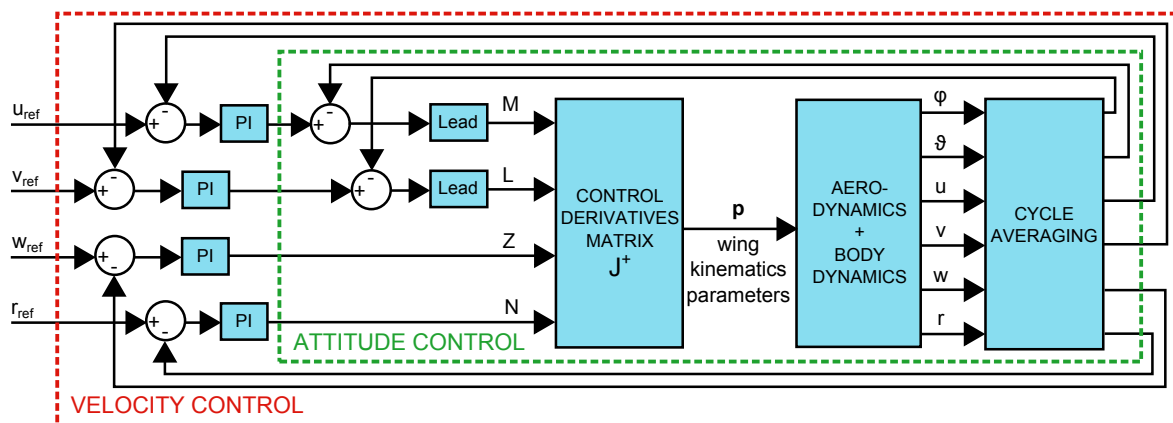

Fig. 9: Cascade control: the inner loop controls attitude, the outer loop controls velocity

Since we develop the controller for a cycle averaged linear system, the best performance is achieved with a discrete design. The sampling frequency is equal to the flapping frequency. The attitude in the inner loop, φ and θ, is controlled by a pair of lead compensators. The velocities in the outer loop, u, v, w and r, are controlled by 4 PI controllers. The control gains were tuned for the linearized system (15) using standard techniques.

3.3. Control derivatives

The forces from the controller are transformed into wing motion by the control derivatives matrix (18). We compute the control derivatives in nearly the same way as the stability derivatives. Since we are around hover we keep the body velocities and angular velocities zero. We chose one parameter, p_i, that we will vary around its equilibrium p_{ei}. All the other parameters are kept in equilibrium $\mathbf{p_e}$. We evaluate the cycle averaged forces and moments for each value. If we plot the averaged forces/moments as a function of the selected parameter, the control derivatives are given by the slopes of tangents to the resulting curves in p_{ei}.

We split the results into two parts. When applying the wing kinematic changes symmetrically on both wings (subscript S) only the longitudinal system forces and moment (X, Z and M) are modified. The linearized relationship can be written as

$$[X, Z, M]^T = \mathbf{J_S}\left[f_S, \phi_{mS}, \phi_{0S}, \alpha_{mS}, \alpha_{0S}, \varphi_{\alpha S}, \delta_{m1S}, \delta_{m2S}, \Theta_S\right]^T \tag{21}$$

To see the importance of each parameter we divide the row belonging to moment by characteristic length R_{CP}. The normalized matrix, with units N/Hz or N/°, is evaluated as

$$
\hat{\mathbf{J}}_{\mathbf{S}} = \begin{array}{c} X \\ Z \\ \frac{M}{R_{CP}} \end{array}
\begin{array}{cccccccccc}
\phi_{mS} & \phi_{0S} & \alpha_{mS} & \alpha_{0S} & \varphi_{\alpha S} & \delta_{m1S} & \delta_{m2S} & \Theta_S & f_S \\
\left[\begin{array}{ccccccccc}
0 & 0.212 & 0 & -1.07 & 0 & 0.107 & 0 & -0.739 & 0 \\
1.21 & 0 & 0.446 & 0 & -0.248 & 0 & 1.18 & 0 & 1.77 \\
0 & -0.519 & 0 & -0.240 & 0 & 0.702 & 0 & -0.192 & 0
\end{array}\right]
\end{array} \tag{22}
$$

For asymmetric changes of wing kinematics (subscript A) only the lateral system force and moments (Y, L and N) are affected. We get

$$[Y, L, N]^T = \mathbf{J}_A\left[\phi_{mA}, \phi_{0A}, \alpha_{mA}, \alpha_{0A}, \varphi_{\alpha A}, \delta_{m1A}, \delta_{m2A}, \Theta_A\right]^T \tag{23}$$

where the control derivatives matrix, normalized as above, is

$$
\hat{\mathbf{J}}_{\mathbf{A}} = \begin{array}{c} Y \\ \frac{L}{R_{CP}} \\ \frac{N}{R_{CP}} \end{array}
\begin{array}{cccccccc}
\phi_{mA} & \phi_{0A} & \alpha_{mA} & \alpha_{0A} & \varphi_{\alpha A} & \delta_{m1A} & \delta_{m2A} & \Theta_A \\
\left[\begin{array}{cccccccc}
-0.288 & 0 & 0.0956 & 0 & 0.401 & 0 & -0.136 & 0 \\
-1.03 & 0 & -0.615 & 0 & 0.176 & 0 & -1.76 & 0 \\
0 & 0.0628 & 0 & -1.63 & 0 & 0.0317 & 0 & -0.828
\end{array}\right]
\end{array} \tag{24}
$$

By studying the matrices above we can identify two groups of parameters according to their effect on generated forces and moments. The first group includes flapping frequency f, sweep amplitude ϕ_m, angle of attack amplitude α_m, phase shift φ_α and amplitude of figure eight-like deviation δ_{m2}. If we modify these parameters symmetrically on both wings, we control the vertical force Z. If we modify these parameters, excluding the flapping frequency, asymmetrically (with positive sign on left wing and with negative sign on right wing) we modulate the L moment (roll) and Y force.

The second group includes sweep angle offset ϕ_0, angle of attack offset α_0, amplitude of oval-like deviation δ_{m1} and mean stroke plane inclination Θ. Symmetric changes of these parameters result into M moment (pitch) and X force modulation. Same parameters taken asymmetrically modify the yaw moment N.

3.4. Choice of control parameters

In the real robot design the number of parameters needed to control the flight needs to be minimized. The matrices (22) and (24) show, that we only need two parameters per wing to generate independently

the four control forces/moments Z, L, M and N. While this approach leaves us no control of the "parasite" forces X and Y, it allows a simpler design of the future robot wing motion mechanism. Another parameter per wing is necessary to assure that X and Y is zero. However, when tested in simulation the controller performance decreased compared to the simpler two parameter per wing controller. Our explanation is that the additional constraints actually reduce the effect of the parameter change on the control force/moment.

For the selected pair of parameters p_1, p_2 we construct a reduced control derivatives matrix

$$\mathbf{J_{red}} = \begin{bmatrix} Z_{p_{1L}} & Z_{p_{1R}} & Z_{p_{2L}} & Z_{p_{2R}} \\ L_{p_{1L}} & L_{p_{1R}} & L_{p_{2L}} & L_{p_{2R}} \\ M_{p_{1L}} & M_{p_{1R}} & M_{p_{2L}} & M_{p_{2R}} \\ N_{p_{1L}} & N_{p_{1R}} & N_{p_{2L}} & N_{p_{2R}} \end{bmatrix} \tag{25}$$

Finally, we transform the control forces/moments into wing kinematic parameters as

$$[p_{1L}, p_{1R}, p_{2L}, p_{2R}]^T = \mathbf{J_{red}}^{-1}[X, L, M, N]^T \tag{26}$$

There are many possible choices of the two control parameters. Since we "ignore" the effect on X and Y forces, full rank of the reduced control derivatives matrix $\mathbf{J_{red}}$ does not guarantee successful control. Moreover we base the control design on the linearized model, while the original system is nonlinear. This requires that the control performance of each combination needs to be tested in nonlinear simulation. In the real robot the final choice of the control parameters will also be constrained by the feasibility of the wing control mechanism design of each choice.

In the next section we present results for ϕ_m and ϕ_0 chosen as control parameters. Their effects on generated force/moments are sketched in Fig. 10.
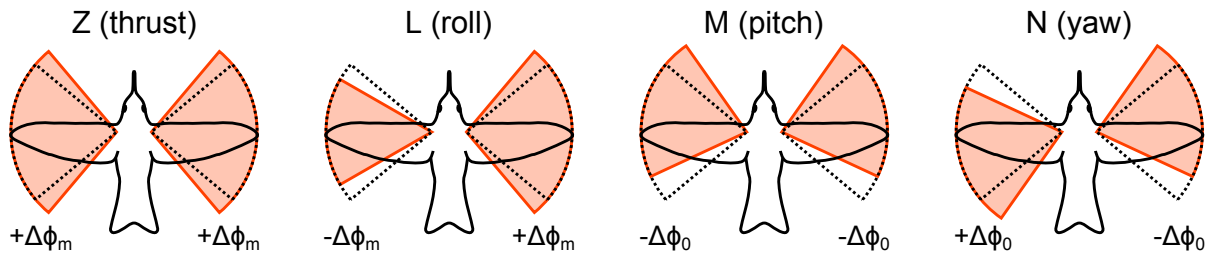

Fig. 10: *Control force and moments generated through wing kinematics parameters ϕ_m and ϕ_0*

4. Simulation results

We evaluated the controller performance by simulations in Matlab/Simulink. The simulation model included nonlinear models of aerodynamics and 6 DOF body dynamics, as described in chapters 2.1.-2.4.. The simulation results are presented for two test trajectories in the four controlled DOFs (velocities u,v,w, angular velocity r). The flight was controlled by the sweep angle amplitude ϕ_m and sweep angle offset ϕ_0.

In the first trajectory we applied a step command in each DOF, one after another, to show the control performance in each single DOF with the coupling effects with the rest of the nonlinear system. The results are in Fig. 11 left. We observe that the longitudinal and vertical dynamics are decoupled from the rest of the system, as indicated by the linearized model. The high frequency oscillation is caused by the pulsating forces due to flapping motion, however the mean values are closely following the linear results. The lateral dynamics and yaw dynamics are coupled, as predicted by the linearization. The control performance in lateral direction is worse than expected, but the system remains stable. The flapping oscillation in lateral and yaw system occurs only when the wing kinematics differs between the wings, but again the mean value follows the command.

The time behavior of the control parameters shows that the necessary changes in wing kinematics are very small. Although the control parameters should be zero in hovering flight according to linearized
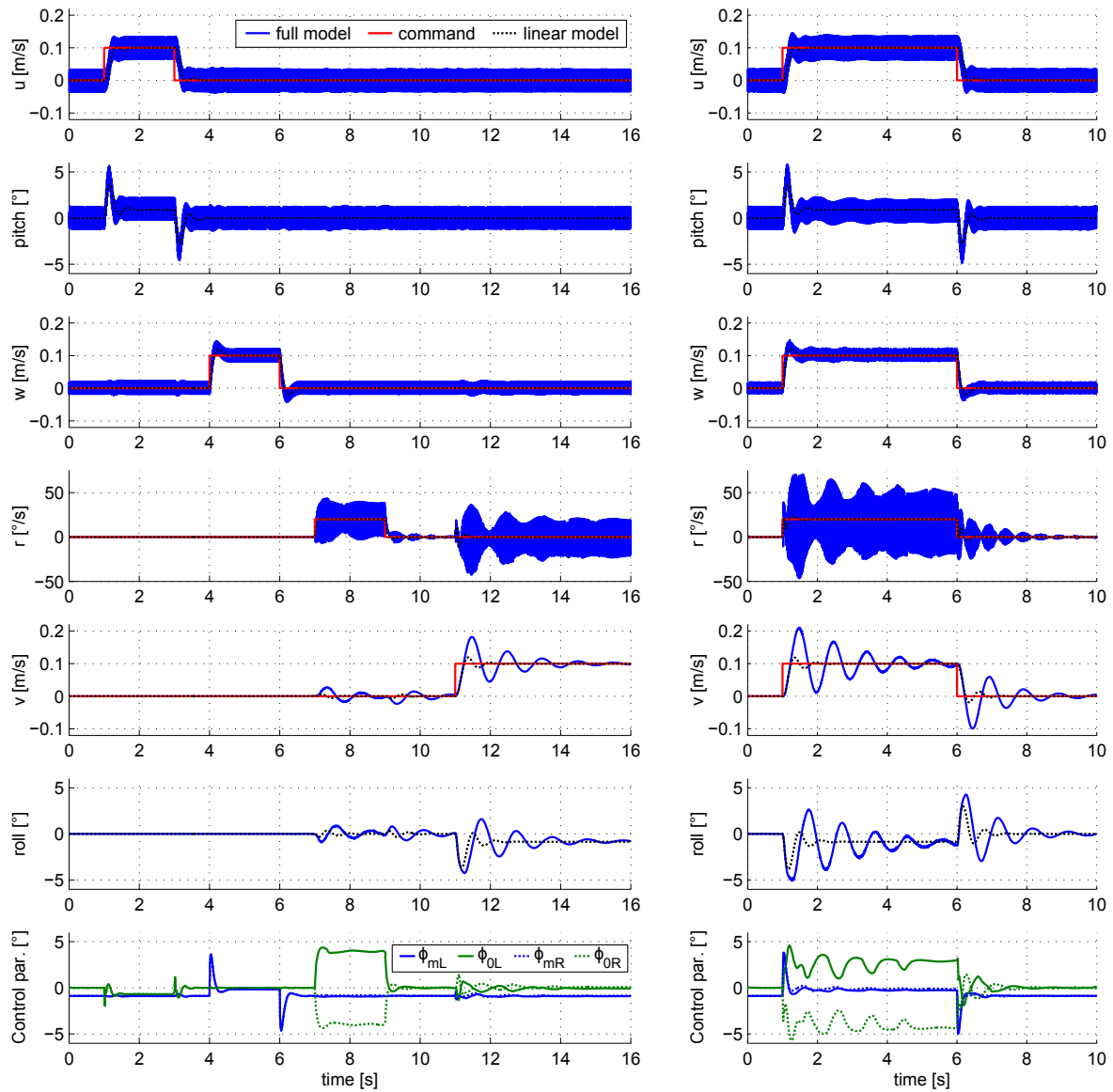
Fig. 11: Step response: step commands one after another for each controlled DOF (left), all step commands at once (right)

model, we observe that sweep amplitude ϕ_m is approximately -1° when all commands are zero. The explanation is that the flapping motion induces a body oscillation that changes the velocity of the wing and subsequently also the angle of attack. This results into slight increase of the cycle averaged lift force that is then compensated by decreasing the sweep amplitude.

The control parameter peaks during the step commands are all below 5° and could be further decreased if the controller was tuned less aggressively. The only exception is the rotation around yaw axis (step in r) during which the sweep offset ϕ_0 remains relatively high (but still below 5°). This is however in accordance with the control derivatives matrix (24), where we can see that the effect of ϕ_0 on yaw moment R is relatively low. A more effective parameter for yaw control may be chosen in future.

In the second trajectory the step command was sent to all the DOFs at once to reveal any control cross-coupling effects and evaluate the potential decrease of control performance. We can see in Fig. 11 right that apart from slight increase of transition times there is no significant change in the overall performance and also the control parameters remain in a similar range.

5. Conclusions

In this paper we presented a simulation model of a hummingbird sized tailless flapping-wing flying robot. The mathematical model was based on rigid body dynamics and quasi steady aerodynamics.

First, we showed by employing system linearization and cycle averaging techniques that the system is decoupled and can be split into separate subsystems for vertical, longitudinal and lateral+yaw dynamics.

Then we parameterized the wing motion and studied the effect of each parameter on the cycle averaged forces. From the results we built a control derivatives matrix. We showed, that the parameters can be split into two groups. The first group parameters can produce a lift force, when changes are applied symmetrically on both wings, and a roll moment, when applied asymmetrically. The second group parameters produce pitch or yaw moments when being modified symmetrically or asymmetrically. Thus, to generate the necessary control force and moments only two wing parameters per wing are necessary. Several choices of the control parameters are possible. The control derivatives matrix was used to transform the control forces and moments into wing motion changes.

Finally, the controller was implemented into the simulation model and tested. We chose sweep (flapping) amplitude and sweep offset (mean wing position) as the control parameters. The controller showed good performance with almost no cross-coupling effects. Apart from lateral dynamics, the nonlinear system response was almost identical with the one of the linearized system. The control performance in sideways flight is decreased, yet still acceptable. The linear approximation of non-linear behavior of lateral dynamics seems to be less precise. A better control of lateral direction flight might be searched in the future.

The results of this study will be further used in the development of the flapping wing robot. We have shown that several choices of the two control parameters are possible. An implementation of these parameters into mechanical design of the robot will be researched in future.

References

Chai, P., Harrykissoon, R., & Dudley, R. (1996) Hummingbird hovering performance in hyperoxic helliox: effects of body mass and sex. *Journal of Experimental Biology*, 199, pp.2745–2755.

Chung, S. & Dorothy, M. (2010) Neurobiologically inspired control of engineered flapping flight. *Journal of Guidance, Control, and Dynamics*, 33, 2, pp.440–453.

de Croon, G., de Clerq, K., Ruijsink, R., Remes, B., & de Wagter, C. (2009) Design, aerodynamics, and vision-based control of the delfly. *International Journal of Micro Air Vehicles*, 1, 2, pp.71–97.

Deng, X., Schenato, L., Wu, W. C., & Sastry, S. S. (2006a) Flapping flight for biomimetic robotic insects: part I-system modeling. *IEEE Transactions on Robotics*, 22, 4, pp.776–788.

Deng, X., Schenato, L., & Sastry, S. (2006b) Flapping flight for biomimetic robotic insects: part II-flight control design. *IEEE Transactions on Robotics*, 22, 4, pp.789–803.

Dickinson, M. H., Lehmann, F.-O., & Sane, S. P. (1999) Wing rotation and the aerodynamic basis of insect flight. *Science*, 284, 5422, pp.1954–1960.

Doman, D. B., Oppenheimer, M. W., & Sigthorsson, D. O. (2010) Wingbeat shape modulation for flapping-wing micro-air-vehicle control during hover. *Journal of Guidance, Control, and Dynamics*, 33, 3, pp.724–739.

Ellington, C. P. (1984). The aerodynamics of hovering insect flight. II. Morphological parameters *Philosophical Transactions of the Royal Society of London. Series B, Biological Sciences*, 305, 1122, pp.17–40.

Keennon, M., Klingebiel, K., Won, H., & Andriukov, A. (2012) Development of the Nano Hummingbird: A Tailless Flapping Wing Micro Air Vehicle. in: *50th AIAA Aerospace Sciences Meeting including the New Horizons Forum and Aerospace Exposition*, pp. 1–24.

Michael, N., Mellinger, D., Lindsey, Q., & Kumar, V. (2010) The grasp multiple micro uav testbed. *IEEE Robotics and Automation*, 17, 3, pp.56–65.

Orlowski, C., Anouck, G., & Shyy, W. (2010). Open loop pitch control of a flapping micro-air vehicle using a tail and control mass. In *2010 American Control Conference, Marriott Waterfront, Baltimore*, pp.536–541.

Orlowski, C. T. & Girard, A. R. (2012) Dynamics, stability, and control analyses of flapping wing micro-air vehicles. *Progress in Aerospace Sciences*, in press.

Padfield, G. D. (2007) *Helicopter Flight Dynamics: The Theory and Application of Flying Qualities and Simulation Modeling*. Blackwell Science Ltd., Washington DC, 2nd edition.

Rakotomamonjy, T., Ouladsine, M. & Le Moing, T. (2010) Longitudinal modelling and control of a flapping-wing micro aerial vehicle. *Control Engineering Practice*, 18, 7, pp.679–690.

Sane, S. P. (2003) The aerodynamics of insect flight. *Journal of Experimental Biology*, 206, pp.4191–4208.

Sane, S. P. & Dickinson, M. H. (2002) The aerodynamic effects of wing rotation and a revised quasi-steady model of flapping flight. *Journal of Experimental Biology*, 205, pp.1087–1096.

Shyy, W., Aono, H., Chimakurthi, S., Trizila, P., Kang, C.-K., Cesnik, C., & Liu, H. (2010) Recent progress in flapping wing aerodynamics and aeroelasticity. *Progress in Aerospace Sciences*, 46, 7, pp.284–327.

Taylor, G. K., Nudds, R. L., & Thomas, A. L. R. (2003) Flying and swimming animals cruise at a Strouhal number tuned for high power efficiency. *Nature*, 425, pp.707–711.

Taylor, G. K. and Thomas, A. L. R. (2002) Animal flight dynamics II. Longitudinal stability in flapping flight. *Journal of Theoretical Biology*, 214, 3, pp.351–370.

Tobalske, B. W., Warrick, D. R., Clark, C. J., Powers, D. R., Hedrick, T. L., Hyder, G. A., & Biewener, A. A. (2007) Three-dimensional kinematics of hummingbird flight. *Journal of Experimental Biology*, 210, 13, pp.2368–2382.

Zhang, Y. & Sun, M. (2010) Dynamic flight stability of a hovering model insect: lateral motion. *Acta Mech. Sinica*, 26, 2, pp.175–190.